PHYSICAL REVIEW B VOLUME 13, NUMBER 12 15 JUNE 1976

Electronic Raman scattering and the metal-insulator transition in doped silicon

Kanti Jain†
Department of Electrical Engineering and Materials Research Laboratory, University of Illinois at Urbana-Champaign, Urbana, Illinois 61801

Shui Lai and Miles V. Klein
Department of Physics and Materials Research Laboratory, University of Illinois at Urbana-Champaign, Urbana, Illinois 61801
(Received 5 May 1975; revised manuscript received 17 November 1975)

We have systematically studied the valley-orbit Raman spectrum of phosphorus-doped silicon for donor concentrations on both sides of the metal-insulator transition. As the impurity concentration n_d increases, the $1s(A_1) \rightarrow 1s(E)$ valley-orbit line broadens rapidly and asymmetrically. The valley-orbit line broadens beyond recognition before n_d reaches n_c, the critical value for the metal-insulator transition. A continuum due to intervalley fluctuations starts appearing as a background as n_d approaches n_c. This continuum becomes stronger with increasing n_d, and above n_c it completely dominates the spectrum. We have also observed some of the above features in antimony- and arsenic-doped silicon. To understand the broadening of the valley-orbit line and to calculate the resulting line shape, we have applied the notion that molecular bonding alters the valley-orbit splitting by estimating the occupancy of donor sites in a two-donor "molecule" treated in the Heitler-London approximation. The continuum starts at zero excitation energy and may be understood as single-particle excitations within a single, partially occupied energy band superimposed on a quasielastic Rayleigh line. The observed temperature dependence of the continuum can be qualitatively understood in terms of temperature-dependent occupation probabilities. For n_d just below n_c the remnant of the valley-orbit line shows a temperature dependence that can be explained by thermal depopulation of the $1s(A_1)$ ground-state orbitals. A sum rule valid for all concentrations has been derived for an integral of the intensity. It shows that the gross features of the spectrum are dominated by the short-range, or intervalley, part of the donor potential. Spectra taken on silicon crystals with arsenic and antimony donors gave results similar to those with phosphorus donors. We have also studied the Raman spectra of several p-type silicon crystals. A low-frequency continuum was observed from boron, gallium, and aluminum impurities, but only boron showed the sharp acceptor line of the B type seen previously.

I. INTRODUCTION

Raman scattering has provided a great deal of information about electronic excitations in semiconductors. In this paper we apply the technique to silicon doped with phosphorus donors. Emphasis is placed on the changes in the donor Raman spectra as the donor concentration is varied to produce the metal-insulator (M-I) transition. Many of the traditional experimental methods for studying this transition, such as transport, electron-spin-resonance, and nuclear-magnetic-resonance measurements, deal with properties of the low-lying electronic excitations near the Fermi level. The Raman effect studies higher excitations and the concentration dependence of both initial and final states. The Si:P system is a good one for Raman studies, since it has the many-valley conduction band necessary for large electronic Raman cross sections, since much is already known about its M-I transition from transport and other measurements, and since the YAlG:Nd^{3+} laser is available to provide photons having an energy just below the indirect band gap.

In the remainder of this section we shall review experimental work on electronic Raman scattering in semiconductors, then some general experimental work on the M-I transition in semiconductors, and finally mention the previous Raman work on this transition. Section II describes some of the experimental techniques, and Sec. III develops the theory of electronic Raman transitions on isolated donors in an indirect semiconductor. Section IV presents our results in Si:P. We begin with dependence on concentration of the Raman spectra. For rising low concentrations one sees the $1s(A)$ to $1s(E)$ valley-orbit line broaden and shift asymmetrically. A model is then introduced that reproduces some of these features qualitatively. At higher concentrations where the material is characterized by impurity-band conduction one observes a broad Raman continuum that starts at zero energy. Some of its features are reproduced by a model in which electrons in a single band make random transitions from states below the Fermi level to states above it. Data will then be presented on the temperature dependence of the spectra for several concentrations. No attempt will be made to provide a general theory of Raman scattering in the heavily doped case, but general expressions will be presented for the cross section in terms of the spectral function

for intervalley density fluctuations. A rather general sum rule will then be derived valid for all concentrations. In terms of it we shall relate the overall strength of the scattering to the strength of the short-range part of the donor potential and to the probability of finding electrons at the donor sites.

In Sec. V we present results on Si doped with As and Sb donors and B, Al, and Ga acceptors. Section VI summarizes our results.

Henry *et al.* reported the first observation of the electronic Raman effect in semiconductors.[1] They observed Raman transitions among acceptor levels in zinc- and magnesium-doped gallium phosphide. Wright and Mooradian observed Raman scattering from phosphorus,[2] arsenic,[3,4] and antimony[3,4] donors in silicon. They reported for Si:P a single valley-orbit Raman transition, $1s(A_1) \rightarrow 1s(E)$, and they showed, using a three-band model and the effective-mass approach, why the $1s(A_1) \rightarrow 1s(T_1)$ transition was not seen. Manchon and Dean observed the $1s(A_1) \rightarrow 1s(E)$ valley-orbit transition for sulphur, selenium, and tellurium donors in gallium phosphide.[5] By performing stress experiments they showed that the $1s(E)$ state was the final state of the transition. Colwell and Klein[6] observed the valley-orbit transition of nitrogen donors in the 6*H* polytype of silicon carbide. Doehler *et al.* observed Raman transitions for gallium acceptors[7] and arsenic donors[7,8] in germanium.

Information about the spectrum of collective modes and single-particle excitations can also be obtained by light-scattering techniques. Single-particle scattering, in which charged carriers are scattered out of the Fermi sea, is a direct measure of the velocity distribution of the carriers, and the polarization characteristics of the Raman-scattered light yield information on the coupling mechanism responsible for the scattering. Mooradian[9] has observed single-particle scattering in *n*-type GaAs, InP, CdTe, and AlSb. The large cross section and the polarization selection rules observed were explained by the spin-density fluctuation mechanism proposed by Hamilton and McWhorter.[10] Scattering by this mechanism was also observed in indium- and gallium-doped CdS,[11,12] and in *p*-type GaAs,[13] and in *p*-type ZnS.[14]

In doped semiconductors the overlap between the wave functions of carriers on neighboring impurity atoms increases with increasing impurity concentration, and the metal-insulator transition takes place at a certain critical concentration n_c. This phenomenon was first observed by Busch and Labhart,[15] who found that the resistivity of silicon carbide showed a rapid drop as the impurity concentration was increased to a critical value. Transport measurements on phosphorus-doped silicon,[16] antimony-,[17,18] phosphorus-, and arsenic-doped germanium,[18] nitrogen-doped silicon carbide,[19] indium antimonide,[20] lead sulphide,[21] and gallium arsenide[22] showed that the *M-I* transition was a general phenomenon in doped semiconductors. Measurements of the Hall coefficient at low temperatures show that the number of free carriers n in a doped semiconductor increases sharply as the impurity concentration approaches a critical concentration n_c; above n_c, n is equal to the impurity concentration.[16-18] The resistivity, when plotted against the impurity concentration, shows a precipitous drop near n_c,[16-18] thus supporting the Hall data.

Sundfors and Holcomb[23] measured the spin-lattice relaxation rate, $1/T_1$, for the ^{29}Si nuclear-spin system in Si:P. They observed that $1/T_1$ showed a rapid decrease in the impurity concentration range between 2.5×10^{18} and 6×10^{18} cm^{-3}. This can be attributed to a delocalization of the electrons in this concentration range, consistent with the value 3×10^{18} cm^{-3} arrived at by transport measurements. Further, the observation that $1/T_1$ is proportional to the temperature for the 6×10^{18} cm^{-3} sample suggested nuclear relaxation by a degenerate system of free electrons. The recent data of Brown and Holcomb[24] on the ^{31}P resonance in Si:P with impurity concentration in the range from 7.5×10^{18} to 8×10^{19} cm^{-3} also support a model in which all the donor electrons participate in a single, interacting system. ESR data[25,26] also point toward a value of n_c in the vicinity of 3×10^{18} cm^{-3} for Si:P. For donor concentrations in the range 7×10^{17}–3×10^{18} cm^{-3} only a single ESR line is seen, and its width decreases with increasing concentration. This suggests that the donor electrons move over larger and larger clusters of donor sites rather than each being bound to an individual donor nucleus. The increase in the width observed for impurity concentrations greater than 3×10^{18} cm^{-3} could presumably be due to lifetime broadening. The Knight-shift data suggest that the Fermi level in Si:P moves into the conduction band as the donor concentration increases beyond 2×10^{19} cm^{-3}.[23] Bethin *et al.*[27] have measured the polarizabilities of Sb, P, and As donors in Si, and find that the static dielectric constant of the doped material diverges in the vicinity of n_c. Marko *et al.*[28] from their specific-heat measurements on heavily doped Si:P find that the system is essentially metallic for impurity concentrations greater than 5.9×10^{18} cm^{-3}, but for smaller concentrations they see evidence of partial localization of the donor electrons.

Raman studies of the metal-insulator transition

in semiconductors have been few. Colwell and Klein[6] observed a continuum extending to roughly 65 meV in heavily doped 6*H* SiC:N and attributed it to overlap between broadened valley-orbit levels. Recently, Doehler *et al.*[8,29] have studied the Ge:As system for a wide range of impurity concentrations and find that the sharp valley-orbit line seen at low concentrations changes to a continuum resembling single-particle scattering at high concentrations. They note, however, that a substantial fraction of the donor electrons appear to remain localized above n_c. Evidence of wave-function overlap in gallium-doped germanium has also been reported.[7,8]

II. EXPERIMENTAL

The optical-absorption coefficient of silicon for wavelengths near 1.064 μm, the output wavelength of a YAlG:Nd laser, shows a minimum for both n- and p-type silicon crystals. Absorption is greater for shorter wavelengths due to the onset of transitions across the indirect gap and for longer wavelengths due to free-carrier absorption, which increases as λ^2. Even at this optimum wavelength our more heavily doped samples gave weak Raman signals. This necessitated the use of counting times as long as 50 sec with output powers of 2–6 W. Such powers resulted in considerable heating of the samples, and we found that it was difficult to cool them below 17 K in our cryostat, a 3-liter Janis Model 8 DT equipped with super Vari-temp for cooling with cold helium gas.

Since the output of the YAlG:Nd laser is unpolarized, a Glan-Thompson prism was employed to select a particular linear polarization. The Raman-scattered light was collected at 90° to the incident direction. Light from the exit slit of the Spex $\frac{3}{4}$-m double monochromator was focused onto the cathode of an Amperex CVP 150 photomultiplier with S-1 response. The monochromator was equipped with gratings ruled at 1200 lines/mm and blazed at 1 μm.

Samples of doped silicon crystals were obtained from several sources. Some were purchased from Semimetals, Inc., Mountain View, Calif., and General Diodes Corp., Framingham, Mass., and other obtained from Streetman, Anner, Sah, and Handler of the University of Illinois, Urbana, Ill., and Gupta of Monsanto Corp., St. Peters, Mo. Resistivity measurements were made at room temperature with a four-point probe on all samples to give their impurity concentrations; mass-spectroscopic analyses showed that the samples had negligible compensation by group-III acceptor impurities.

Optical-absorption measurements were made on many of the samples at both room and helium temperatures. The room-temperature data were taken using a Gary 14 spectrophotometer and are shown in Fig. 1(a). In Fig. 1(b) we show low temperature data taken at 17 K using a Zeiss PM QII spectrophotometer. From the latter data we see that the measured absorption coefficients at 1.06 μm ranged from less than 4 cm^{-1} for the most lightly doped samples to approximately 10 cm^{-1} for the most heavily doped ones, indicating that the optical penetration depth was of the order of a millimeter.

Most samples measured $3\times3\times13$ mm^3; the longest edge was oriented along ⟨100⟩ and the others along ⟨110⟩. Orientation was done by using the Laue back reflection technique. All samples were mechanically polished to 0.05 μm. Various $HF\text{-}HNO_3$ systems were tried for chemical etching but no difference was observed between the spectra obtained from etched and unetched samples.

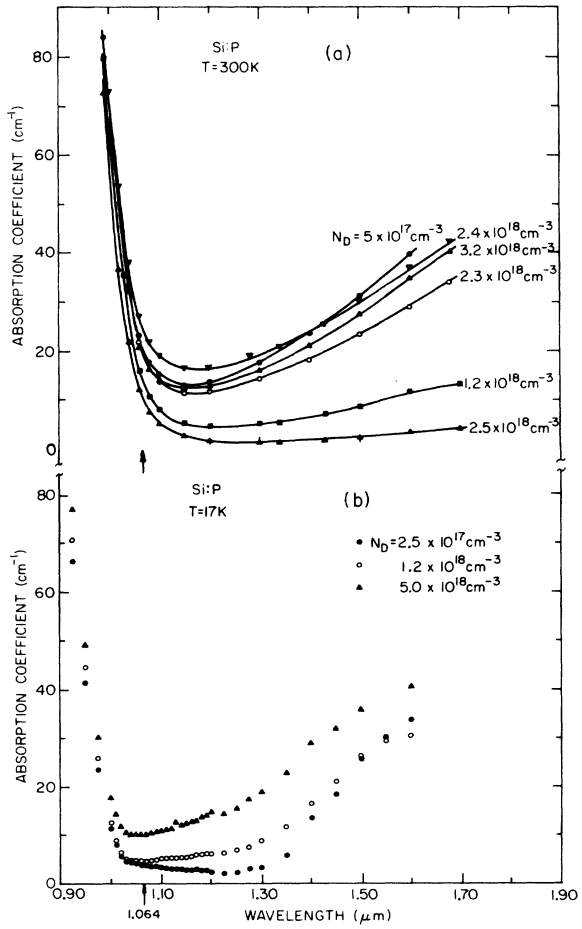

FIG. 1. Absorption coefficient of Si:P at 300 and 17 K. The arrow denotes the wavelength of the YAlG:Nd laser line.

III. THEORY OF DONOR RAMAN TRANSITIONS

In the Raman scattering process an incident photon in a state with energy $\hbar\omega_L$, polarization direction $\vec{\eta}_L$, and wave vector $\vec{k}_L$ scatters to a state $(\hbar\omega_R, \vec{\eta}_R, \vec{k}_R)$ and the system goes from an initial state of energy E_i to a final state of energy E_f through the creation or destruction of an elementary excitation. Energy conservation requires

$$\hbar(\omega_L - \omega_R) = E_f - E_i = \pm\hbar\omega . \tag{1}$$

The Hamiltonian describing the interaction of radiation with a system of N electrons is given by

$$H = \sum_{i=1}^{N} \frac{1}{2m}\left[\vec{p}_i - (e/c)\vec{A}(\vec{r}_i, t)\right]^2 + V(\vec{r}_1, \vec{r}_2, \ldots, \vec{r}_N) = H_0 + H_1 + H_2 , \tag{2}$$

where

$$H_0 = \sum_{i=1}^{N} \frac{p_i^2}{2m} + V(\vec{r}_1, \vec{r}_2, \ldots, \vec{r}_N) , \tag{3}$$

$$H_1 = \sum_{i=1}^{N} \frac{e}{2mc}\left[\vec{p}_i \cdot \vec{A}(\vec{r}_i, t) + \vec{A}(\vec{r}_i, t)\cdot \vec{p}_i\right] , \tag{4}$$

and

$$H_2 = \sum_{i=1}^{N} \frac{e^2}{2mc^2} A^2(\vec{r}_i, t) . \tag{5}$$

We use the effective-mass approximation to treat the donor levels. The donor electron is assumed to have the effective mass m^* of a conduction-band minimum. Kohn[30] has shown that for v equivalent minima the donor electron wave function can be written

$$\psi_n^{(\gamma)}(\vec{r}) = \sum_{j=1}^{v} \alpha_j^{(\gamma)} \phi_j(\vec{r}) F_j^n(\vec{r}) . \tag{6}$$

Here $\phi_j(\vec{r}) = u_j(\vec{r})\, e^{i\vec{k}\cdot\vec{r}}$ is the Bloch function at the jth minimum, $\alpha_j^{(\gamma)}$ are certain numerical coefficients that depend on the point-group symmetry of the impurity Hamiltonian, and γ labels the irreducible representation of the group we are considering. The $F_j^n(\vec{r})$ are hydrogenic envelope functions that are slowly varying on the scale of a lattice constant. They obey the effective-mass wave equation

$$\left(\sum_{\alpha\beta} \frac{1}{2m}\mu_{\alpha\beta}^{(j)} p_\alpha p_\beta + [U(\vec{r}) - E]\right) F_j^n(r) = 0 , \tag{7}$$

where we have neglected the spin-orbit interaction. $U(\vec{r}) = e^2/\epsilon_s r$ is the statically screened Coulomb potential of the donor and the eigenvalue E is the energy relative to the conduction-band minimum. We denote $\mu_{\alpha\beta}^{(j)}$ as $(m/m^*)_{\alpha\beta}$ for valley j.

To calculate the scattering cross section,[4,6,31] we use the H_2 term in first order and the H_1 term in second order. In dipole approximation the Raman cross section can be written

$$\frac{d\sigma(0\to f)}{d\Omega_R} = \left(\frac{e^2}{mc^2}\right)^2 \frac{\omega_R}{\omega_L} \left| \left(\vec{\eta}_L \cdot \vec{\eta}_R \langle f|0\rangle + \frac{1}{m}\sum_m \frac{\langle f|\vec{\eta}_R\cdot\vec{p}|m\rangle\langle m|\vec{\eta}_L\cdot\vec{p}|0\rangle}{E_0 - E_m + \hbar\omega_L} \frac{\langle f|\vec{\eta}_L\cdot\vec{p}|m\rangle\langle m|\vec{\eta}_R\cdot\vec{p}|0\rangle}{E_0 - E_m - \hbar\omega_R}\right)\right|^2 . \tag{8}$$

To evaluate the sum over m in Eq. (8) we use a simple two-band model for the semiconductor in which the conduction band has energy E_c at its jth minimum at k_j and the valence band has energy E_v at k_j. The direct gap at k_j is E_G. In this model three kinds of Raman transition can take place: (i) the donor electron goes from the $1s$ ground state to a higher $1s$ level via a virtual transition to the valence band; (ii) the electron goes from the ground state to a higher hydrogenic state, say, $2s$, again via a virtual transition to the valence band; and (iii) the electron goes from the ground state to an excited $1s$ state (or some other evenparity state) via a virtual transition to an odd-parity hydrogenic state, e.g., a $2p$ state. It can be shown that processes (ii) and (iii) are relatively unimportant in comparison to process (i).[6,31] Putting $E_m = E_v$ and approximating E_0 by E_c, we reduce the sum over m in Eq. (8) to

$$\sum_m = \sum_{\alpha\beta} \eta_L^\alpha \eta_R^\beta \left(\frac{\langle f|p_\alpha p_\beta|0\rangle}{E_G - \hbar\omega_R} + \frac{\langle f|p_\alpha p_\beta|0\rangle}{E_G + \hbar\omega_L}\right) . \tag{9}$$

Using the form (6) for the initial and final donor electron wave functions, $\psi_0^{(\lambda)}(\vec{r})$ and $\psi^{(\delta)}(\vec{r})$, respectively, we write Eq. (9) as

$$\sum_m = \sum_{\alpha\beta} \eta_L^\alpha \eta_R^\beta \sum_j \alpha_j^{(\gamma)*} \alpha_j^{(\omega)} \left(\frac{\langle u_j|(\vec{p}+\hbar\vec{k}_j)_\alpha (\vec{p}+\hbar\vec{k}_j)_\beta|u_j\rangle}{E_G - \hbar\omega_R} + \frac{\langle u_j|(\vec{p}+\hbar\vec{k}_j)_\beta (\vec{p}+\hbar\vec{k}_j)_\alpha|u_j\rangle}{E_G + \hbar\omega_L}\right)\langle F_j^f|F_j^0\rangle , \tag{10}$$

where $\alpha_j^{(0)}$ and $\alpha_j^{(f)}$ are the Kohn-Luttinger coefficients that appear in the effective-mass wave functions of the initial and final states. Since the envelope functions $F_j^n(\vec{r})$ are slowly varying, we have assumed that the momentum operator $\vec{p}$ does not act on them. The presence of the overlap integral $\langle F_j^f | F_j^0 \rangle$ in Eq. (10) shows that the Raman transitions must be within the $1s$ manifold only.

Now we use the definition of the effective-mass tensor

$$\left(\frac{m}{m^*}\right)_{\alpha\beta} = \delta_{\alpha\beta} + \frac{2}{m}\sum_{l\neq 0}\frac{\langle u_j|(\vec{p}+\hbar\vec{k}_j)_\alpha|u_j^l\rangle\langle u_j^l|(\vec{p}+\hbar\vec{k}_j)_\beta|u_j\rangle}{E_0(\vec{k}_j)-E_l(\vec{k}_j)} \tag{11}$$

and the approximation $\hbar(\omega_L-\omega_R)\ll E_G$ to write, at $T=0$, the cross section in Eq. (8) as

$$\frac{d\sigma(0\to f)}{d\Omega_R} = r_0^2\frac{\omega_R}{\omega_L}\left|\sum_{\alpha\beta}\eta_L^\alpha\eta_R^\beta\left\{\sum_j \alpha_j^{(f)*}\alpha_j^{(0)} + \frac{E_G^2}{E_G^2-(\hbar\omega_L)^2}\sum_j \alpha_j^{(f)}\alpha_j^{(0)}\left[\left(\frac{m}{m^*}\right)_{\alpha\beta}^{(j)} - \delta_{\alpha\beta}\right]\right\}\right|^2, \tag{12}$$

where $r_0 = e^2/mc^2$ is the classical radius of the electron.

Equation (12) can be simplified further by using the following form for the effective-mass tensor for the case of axial symmetry:

$$(\vec{m}/m^*)^{(j)} = \vec{\mu}_j = \mu_\perp\vec{I} + (\mu_\parallel - \mu_\perp)\hat{\eta}_j\hat{\eta}_j . \tag{13}$$

Here $\hat{\eta}_j$ is a unit vector along the axis of the jth valley. With the use of Eq. (13), Eq. (12) can be written

$$\frac{d\sigma(0\to f)}{d\Omega_R} = r_0^2\frac{\omega_R}{\omega_L}\left|\vec{\eta}_L\cdot\left(\left[1+(\mu_\perp-1)R_{12}\right]\sum_j \alpha_j^{(f)*}\alpha_j^{(0)}\vec{I} + R_{12}(\mu_\parallel-\mu_\perp)\times\sum_j \alpha_j^{(f)*}\alpha_j^{(0)}\hat{\eta}_j\hat{\eta}_j\right)\cdot\vec{\eta}_R\right|^2, \tag{14}$$

where $R_{12} = E_G^2/[E_G^2-(\hbar\omega_L)^2]$ is the resonance enhancement factor. For Raman scattering ($f\neq 0$) the first term in the large parentheses in Eq. (14) vanishes and we obtain

$$\frac{d\sigma(0\to f)}{d\Omega_R} = r_0^2\frac{\omega_R}{\omega_L}R_{12}^2(\mu_\parallel-\mu_\perp)^2\times\left|\sum_j \alpha_j^{(f)*}\alpha_j^{(0)}(\vec{\eta}_L\cdot\hat{\eta}_j)(\vec{\eta}_R\cdot\hat{\eta}_j)\right|^2. \tag{15}$$

In addition there will be Rayleigh scattering ($f=0$) with cross section

$$\frac{d\sigma}{d\Omega} = r_0^2\frac{\omega_R}{\omega_L}(\vec{\eta}_L\cdot\vec{\eta}_R)^2\left|(1-R_{12})+R_{12}\mu_{av}\right|^2, \tag{16}$$

where $\mu_{av} = \frac{1}{2}\mu_\parallel + \frac{2}{3}\mu_\perp$.

We calculate the Raman cross section for shallow donors in silicon. In silicon there are six equivalent conduction-band minima located along the $\langle 100\rangle$ directions at about 82% of the distance to the Brillouin zone boundary.[32] The ground state of the donor electron will be sixfold degenerate in the effective-mass approximation, but, when corrections are taken into account, part of this sixfold degeneracy is lifted. The remaining degeneracy can be obtained solely from the symmetry of the donor electron Hamiltonian. For substitutional donors the impurity Hamiltonian is invariant under the tetrahedral group T_d and the donor ground state splits into a nondegenerate, fully symmetric $1s(A_1)$ level, a doubly degenerate $1s(E)$ level and a triply degenerate $1s(T_1)$ level. The coefficients $\alpha_j^{(\gamma)}$ that appear in the wave functions (Eq. (6)) of the states in the $1s$ manifold are given by Kohn[30] as

$$\begin{aligned}
\alpha_j^{(A1)} &= (1/\sqrt{6})(1,\ 1,\ 1,\ 1,1,\ 1),\\
\alpha_j^{(E-1)} &= \tfrac{1}{2}(1,\ 1,\ -1,\ -1,\ 0,\ 0),\\
\alpha_j^{(E-2)} &= (1/2\sqrt{3})(1,\ 1,\ 1,\ 1,\ -2,\ -2),\\
\alpha_j^{(T1-1)} &= (1/\sqrt{2})(1,\ -1,\ 0,\ 0,\ 0,\ 0),\\
\alpha_j^{(T1-2)} &= (1/\sqrt{2})(0,\ 0,\ 1,\ -1,\ 0,\ 0),\\
\alpha_j^{(T1-3)} &= (1/\sqrt{2})(0,\ 0,\ 0,\ 0,\ 1,\ -1).
\end{aligned} \tag{17}$$

The Raman cross section for a transition from the $1s(A_1)$ ground state to an excited state can now be readily calculated by use of Eqs. (15) and (17). We find that the tensors

$$\vec{T}_f = \sum_i \alpha_i^{(f)*}\alpha_i^{(0)}\hat{n}_i\hat{n}_i \tag{18}$$

for transitions to $1s(E-1)$ and $1s(E-2)$ are

$$T_{E-1} = \begin{pmatrix} \frac{1}{2}\sqrt{3}\,a & 0 & 0\\ 0 & -\frac{1}{2}\sqrt{3}\,a & 0\\ 0 & 0 & 0\end{pmatrix}$$

and

$$T_{E-2} = \begin{pmatrix} \frac{1}{2}a & 0 & 0\\ 0 & \frac{1}{2}a & 0\\ 0 & 0 & -a\end{pmatrix}, \tag{19}$$

where

$$a = \tfrac{1}{3}\sqrt{2} \ . \tag{20}$$

In the standard E-polarization geometry—$\vec{\eta}_L \| [1\bar{1}0]$ and $\vec{\eta}_R \| [110]$—the Raman cross section is

$$\frac{d\sigma}{d\Omega} = \tfrac{1}{6} r_0^2 \frac{\omega_R}{\omega_L} R_{12}^2 (\mu_\parallel - \mu_\perp)^2 . \tag{21}$$

The cross section for transitions to the $1s(T_1)$ states is zero. Thus, in the effective-mass approximation, only one valley-orbit Raman transition—$1s(A_1) \rightarrow 1s(E)$—is observable.

IV. RESULTS AND DISCUSSION: Si:P SAMPLES

A. Dependence upon concentration

In Figs. 2 (a)–(j) we show the Raman spectra of Si:P crystals in the 0–200-cm^{-1} region as a function of impurity concentration. About 5.5 W of laser power were used for samples in Figs. 2 (a)–(g), but only 2.4 W for those in Figs. 2 (h)–(j). The spectrum in Fig. 2(a) for $n_d = 7\times10^{16}$ cm^{-3} shows a single sharp line at 105 cm^{-1} caused by the $1s(A_1)$-$1s(E)$ valley-orbit transition of the donor electron. Figures 2 (b)–(f) show that this line broadens rapidly and asymmetrically with increasing donor concentration. Simultaneously a new continuous spectrum appears as a background [Figs. 2 (e)–(j)] that grows stronger and eventually dominates the spectrum. We observe that the valley-orbit peak shifts towards lower energies as the donor concentration increases. From 105 cm^{-1} at $n_d = 7\times10^{16}$ cm^{-3}, it moves to 85 cm^{-1} at $n_d = 2.3\times10^{18}$ cm^{-3}. At $n_d = 2.4\times10^{17}$ cm^{-3} the valley-orbit line is ill defined and for $n_d = 3.2\times10^{18}$ cm^{-3} it shows up only as a knee at 85 cm^{-1}. For $n_d = 5\times10^{18}$ cm^{-3} the knee has moved to 55 cm^{-1}. Spectra taken with polarized incident light and analyzed scattered light show that the continuum has the same symmetry E as the sharp valley-orbit line. It is interesting to compare our results with similar Raman data taken on arsenic-doped germanium.[8] In the latter case, the valley-orbit line broadens less rapidly, it persists more deeply into the metallic regime, and it shifts more slowly towards lower energies with increasing impurity concentration.

A detailed understanding of the change in the shape of the valley-orbit Raman line with increasing concentration requires detailed information about overlap between the wave functions of electrons on neighboring donors. As this overlap increases with increasing impurity concentration, the orbit of an electron spans more and more donor atoms. We expect that its amplitude for being in a central cell will decrease and result in a decrease in the valley-orbit splitting. In the next few paragraphs we briefly sketch a theory based on this concept for calculating the Raman line shape. In Fig. 3 we compare the dependence of the width of the valley-orbit Raman line on n_d with that of $\log_{10}\rho$ and $\log_{10}\epsilon_2$, where ρ is the re-

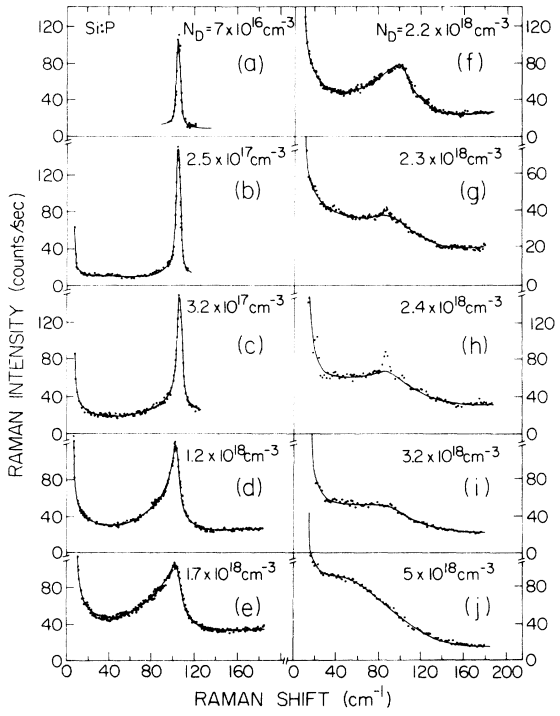

FIG. 2. Stokes Raman spectra of Si:P for various donor concentrations. Actual temperatures were estimated by a thermocouple and by ratios of Stokes to anti-Stokes Raman spectra and were about 21 K for part (a), 30 K for parts (b), (c), (h), (i), (j), 40 K for part (d), 45 K for part (e), and 50 K for parts (f) and (g). The small peak at 84 cm^{-1} in (g) and (h) is a fluorescence line from the YAlG : Nd laser. The scattering geometry was z(all, all)y, with $\vec{x} \| [100]$, $\vec{y} \| [011]$, and $\vec{z} \| [0\bar{1}1]$.

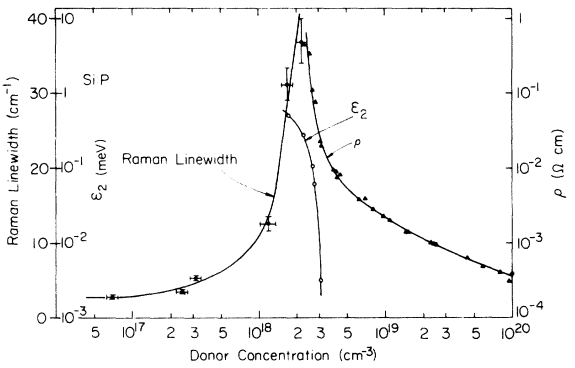

FIG. 3. Width of the valley-orbit Raman line as a function of donor concentration. The values of ρ and ϵ_2 are those of Ref. 16.

sistivity[16] and the activation energy ϵ_2 is often known as the Hubbard gap.[33,34] We note that the Raman line broadens beyond recognition before the resistivity takes on metallic values or before ϵ_2 vanishes. This observation should again be compared with the results for Ge:As,[8] where the valley-orbit line continues to have a measurable width in the metallic ρ regime.

B. Line shape in insulating regime

From Eqs. (6) and (17) it is seen that only in the fully-symmetric $1s(A_1)$ state is the wavefunction nonzero at the donor site ($r=0$). Thus only in this state does the electron experience the departure of the true donor potential from the screened Coulomb potential used in the effective-mass theory [Eq. (7)]. The valley-orbit splitting $E_{\rm VO}$ is a consequence of the fact that the $1s(A_1)$ state is pulled down from the other $1s$ states because it has a finite amplitude at the donor nucleus. The others do not, and their energy is quite close to that given by the effective-mass approximation. Thus, to calculate the line shape of the valley-orbit Raman transition in the insulating regime, we use the notion that the $1s(A_1)$-$1s(E)$ splitting is directly proportional to $|\psi(0)|^2$. To relate this dependence to donor concentration, we visualize the aggregate of donor atoms as a collection of pairs, consisting of a given atom and its nearest neighbor. We treat each pair as a "hydrogen" molecule. We use the Heitler-London method to get the amplitude for the two electrons being at the two nuclei, and therefore obtain $E_{\rm VO}$ as a function of the interdonor distance, R. The line shape can then be calculated by using an appropriate probability distribution for R.

The Heitler-London wave function for the singlet state of two electrons on a pair of donor nuclei is given by

$$\psi(r_1,r_2)=[2(1+S^2)]^{-1/2}\ [\psi_A(r_1)\,\psi_B(r_2)+\psi_A(r_2)\,\psi_B(r_1)]\ . \tag{22}$$

Here $\psi_i(r_1)$ is the Kohn-Luttinger effective-mass wave function for electron 1 on nucleus i and S is the overlap integral

$$S=\langle\psi_A(r)|\psi_B(r)\rangle\ . \tag{23}$$

We are interested in evaluating the expectation value of the operator for the electron density at the two nuclei:

$$\rho(R_A,R_B)=\delta(r_1-R_A)+\delta(r_1-R_B)+\delta(r_2-R_A)+\delta(r_2-R_B)\ . \tag{24}$$

Using Eq. (22) we get

$$\langle\psi(r_1,r_2)|\rho(R_A,R_B)|\psi(r_1,r_2)\rangle=[2/(1+S^2)]\{|\psi(0)|^2+|\psi(R)|^2+S[\psi(0)\,\psi(R)^*+\psi(0)^*\,\psi(R)]\}\ , \tag{25}$$

where $R=|R_A-R_B|$. In the "atomic" case, where the impurity atoms are isolated, the two-electron wave function is $\psi_A(r_1)\,\psi_B(r_2)$ and the corresponding expectation value of the electron density operator at the two nuclei is $2|\psi(0)|^2$. Hence, the ratio of the valley-orbit splitting in the molecular case $E_{\rm VO}(m)$ to that in the atomic case $E_{\rm VO}(a)$ can be written

$$B(R)=\frac{E_{\rm VO}(m)}{E_{\rm VO}(a)}=\frac{|\psi(0)|^2+|\psi(R)|^2+S[\psi(0)\,\psi(R)^*+\psi(0)^*\,\psi(R)]}{(1+S^2)|\psi(0)|^2}\ . \tag{26}$$

Now we write the effective-mass wave function $\psi(r)$ in Eq. (6) in the form

$$\psi(r)=\sum_j \alpha_j F(r)\,u(r)\,e^{i\vec{k}_j^0\cdot\vec{r}}\ . \tag{27}$$

We thus assume that the envelope function $F(r)$ and the periodic part of the Bloch function $u(r)$ do not depend on the valley index j. Then, using the relations $u(R)=u(0)$ and $F(R)=F(0)e^{-R/a_0}$, where a_0 is an appropriate Bohr radius, we get

$$B(R)=[1+G(R)^2+2G(R)\,S(R)]/[1+S(R)^2]\ , \tag{28}$$

where

$$G(R)=\frac{1}{v}\,e^{-R/a_0}\sum_{j=1}^{v}\cos(\vec{k}_j^0\cdot\vec{R}) \tag{29}$$

and

$$S(R)=1+R/a_0+(R^2/3a_0^2)\ G(R)\ . \tag{30}$$

We have calculated the quantity B as a function of R for three orientations of the interdonor axis, along $\langle 111\rangle$, $\langle 110\rangle$, and $\langle 100\rangle$.[35] We have used $a_0=20$ Å, $v=6$, and $k^0=0.82(2\pi/a)=0.95$ Å^{-1}, $a=5.42$ Å being the lattice constant of silicon. Our results are shown in Fig. 4 for the $\langle 111\rangle$ direction. We see that $B(R)$ oscillates rapidly due to the presence of the cosine terms in $G(R)$ [Eq. (29)]. In Fig. 4 we also show the nearest-neighbor probability distribution,[36] $P(R)$, for two donor concentrations. We observe that as the donor concentration increases, the peak of the function $P(R)$ overlaps more with the region where $B(R)$ is less than unity, and therefore, the tail on the lower-energy side of the valley-orbit transition becomes stronger with increasing impurity concentration. In the region where $B(R)>1$, $P(R)$

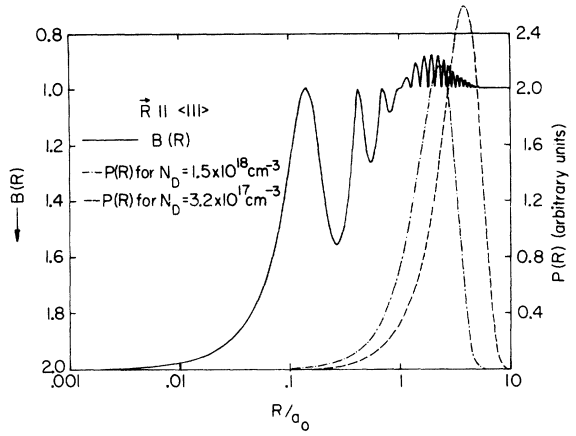

FIG. 4. The function $B(R)$ from Eq. (28) as a function of interdonor distance for $\vec{R}$ along $\langle 111 \rangle$. The probability distribution $P(R)$ is also shown.

is very small. Thus the tail on the higher-energy side will be very weak. To estimate the line shape of the valley-orbit transition we proceed as follows. From Eq. (26), we calculate $E_{VO}(m,R)$ for a given R. Then $P(R)$ gives the intensity of the line at that energy. This is repeated for an appropriate range of R for which $P(R)$ is significant. The line shape is proportional to $I(\omega)=\sum_R P(R)\,\delta(\omega - E_{VO}(m,R))$. Our results for the direction of $\vec{R}$ along $\langle 111 \rangle$ are shown in Fig. 5. The asymmetric broadening with rising donor concentration is clearly seen. The cutoff at 92 cm^{-1} is due to the minimum in $B(R)$ apparent from Fig. 4. It is an artifact of the oversimplified nature of this calculation. The calculated widths are narrower than those experimentally observed by almost a factor of 3, but the main features of the valley-orbit line shape are qualitatively explained. A more complete calculation would average over all directions of $\vec{R}$, but we do not believe that this would alter the results in Fig. 5 by very much. The next step would seem to include overlap within clusters of three or more donor atoms.

A more correct calculation would require the construction of a Heitler-London wave function analogous to Eq. (22) for the excited state of the two-donor "molecule" in which one of the atomic orbitals is $1s(A_1)$ and other is a mixture of $1s(E-1)$ and $1s(E-2)$. The valley-orbit splitting would then be the difference between the expectation value of the Hamiltonian between these two wave functions. The start of such a calculation has been made.[35]

C. Continuum

The continuum that appears at high donor concentrations [shown in Figs. 2 (e)–(j)] is a spectrum of intervalley electron density fluctuations.[37–39] The expression for the scattering cross section due to this mechanism will be given below. It depends on the fact that the effective mass aniso-

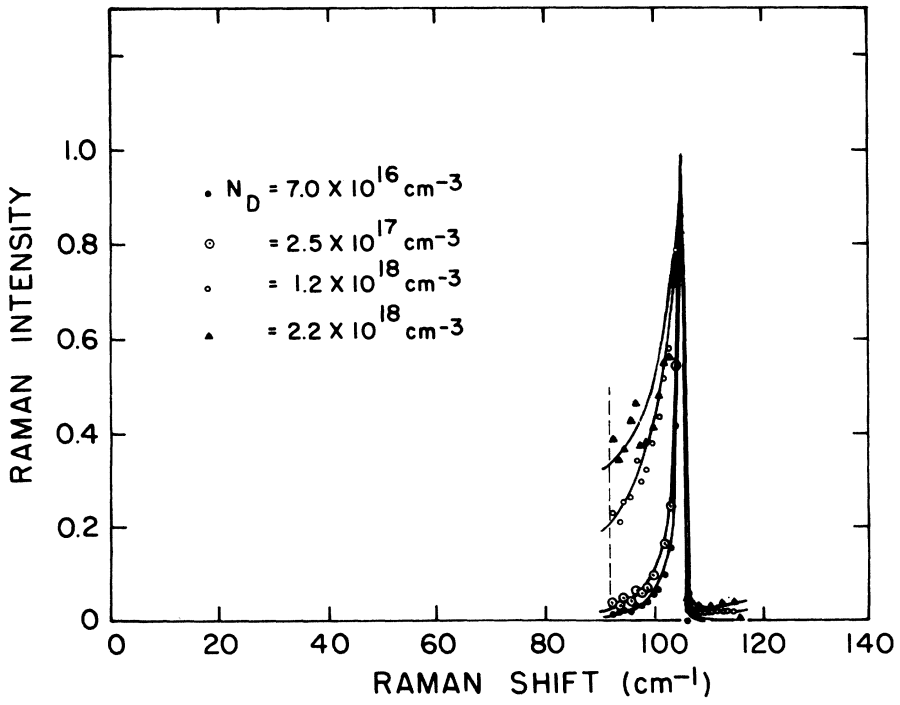

FIG. 5. Valley-orbit line shape calculated for $\vec{R}$ along $\langle 111 \rangle$.

tropy allows electrons in the several valleys to couple in several ways to the incident and scattered radiation fields. A relative density fluctuation among valleys may be excited without exciting a net density fluctuation. The resulting response is not screened by the Coulomb interaction among electrons, since in the random-phase approximation this interaction couples only to a net density fluctuation. This intervalley scattering mechanism produces a light-scattering spectrum of the same symmetry E as that of the valley-orbit Raman line. This is consistent with our experimental observations and is also consistent with the earlier results on SiC:N[6], and Ge:As.[8,29]

Since the continuum starts at zero excitation energy, if single-particle excitations are responsible for it, the energy bands of the initial and final states must overlap. Let us imagine a single, partially filled, band within which the continuum transitions occur. We assume that the disorder produced by the random distribution of donors has negated all selection rules so that an initial state (with energy E) has the same "random access" to any final state (with energy $E+\omega$). If $\rho(E)$ is the density of states in the band, the light-scattering intensity is then proportional to

$$I(\omega)=\int \rho(E)f(E)\rho(E+\omega)[1-f(E+\omega)]\,dE\,. \tag{31}$$

Here $f(E)=(e^{\beta(E-E_f)}+1)^{-1}$ is the Fermi function. We have evaluated Eq. (31) using $E_f=0$ and a Gaussian density of states

$$\rho(E)=e^{-2E^2/\omega_0^2}, \tag{32}$$

where $\omega_0=82$ cm^{-1}. Figure 6 shows the results for five temperatures. The $T=\infty$ curve is simply the Gaussian $e^{-(\omega/\omega_0)^2}$. The calculated curves for 20 and 50 K should be compared with the data of Fig. 2(j) for $n_d=5\times10^{18}$ cm^{-3}. When one subtracts a symmetric central peak from the experimental data, there will remain a definite maximum at about 40 cm^{-1}, and the general appearance will be that of the 20- or 50-K calculated curves.

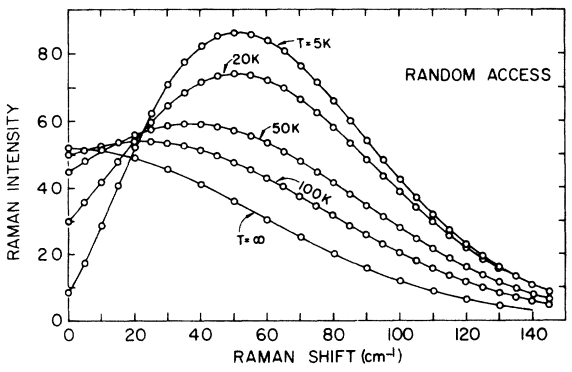

FIG. 6. Raman intensity due to single-particle excitations with random access in a Gaussian band.

The shape of the curves of Fig. 6 is not an artifact of the random-access, single-particle model used to generate them. An exact theory will produce a similar result, for the following reason. The Raman intensity $I(\omega)$ must obey the fluctuation-dissipation theorem for Raman scattering,[40,41] which expresses $I(\omega)$ in the form

$$I(\omega)=[1+n(\omega)]\,\mathrm{Im}R(\omega)\,, \tag{33}$$

where $R(\omega)$ is an appropriate response function and where $n(\omega)$ is the Planck function. One can show that the imaginary part of $R(\omega)$ must be an odd function of ω. At $T=0$ $[1+n(\omega)]$ behaves like a unit step function at $\omega=0$. Thus if the leading term in a power series expansion of ImR in ω is the linear term, the Raman intensity will be proportional to ω for ω small and positive. ImR will eventually decrease, thus producing a maximum in $I(\omega)$.

We believe that the observed Raman spectrum for the 5×10^{18} sample in Fig. 2(j), including the knee at 55 cm^{-1}, can be understood in terms of these general properties of a Raman continuum. It is not necessary to assume that the knee is caused by valley-orbit Raman transitions on isolated donors that still exist in insulating regions above the metal-insulator transition.

D. Temperature dependence

In Fig. 7 we show spectra taken on our most heavily doped sample at true temperatures of 50 K and higher. Each curve is arbitrarily normalized to its value at 23 cm^{-1}. The low-energy part of

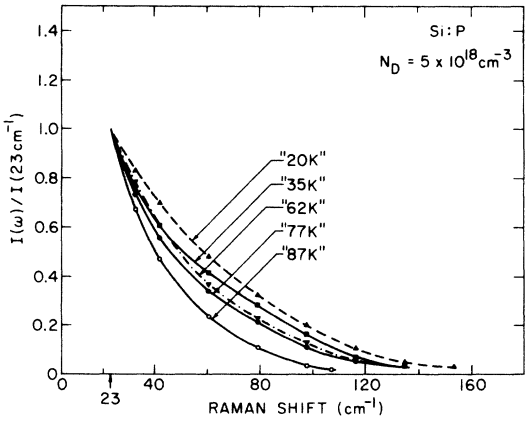

FIG. 7. Temperature dependence of the Raman spectra for $n_d=5\times10^{18}$ cm^{-3}. The spectra were normalized at 23 cm^{-1}. Temperatures are those measured with a thermocouple; the "20 K" sample was actually at about 50 K.

the continuum grows with increasing temperature, and the entire curve shifts to lower energy. The random access model of Fig. 6 mimics this behavior well, if one imagines that the additional Rayleigh component grows with increasing temperature. It is possible that the Rayleigh component is at least partially inelastic. This could be explained as follows. Suppose that there is a remnant of isolated donor behavior to the extent that there is a doubly degenerate $1s(E)$ band higher in energy than the $1s(A)$ band. As the temperature rises, the former will be thermally populated at the expense of the latter. Transitions of the type $1s(E-1)$ to $1s(E-2)$ will be quasielastic and have both A_1 and E symmetry.

In Figs. 8 and 9 we show the Stokes and anti-Stokes Raman spectra taken at two different temperatures on the samples with $n_d = 2.4\times10^{18}$ and 3.2×10^{18} cm^{-3}, respectively. We observe that at higher temperature, the remnant of the valley-orbit peak for the $n_d = 2.4\times10^{18}$-cm^{-3} sample is much weaker, whereas for the $n_d = 3.2\times10^{18}$-cm^{-3} sample it is totally absent. This weakening of the valley-orbit scattering with increasing temperature can at once be interpreted as depletion of the $1s(A_1)$ ground state. Figure 10 shows similar data on the $n_d = 5\times10^{18}$-cm^{-3} sample at three different temperatures. Here the knee at 55 cm^{-1} seen at 30 K vanishes at 62 K. If we assume that the spectrum in the metallic regime (to which the sample in Fig. 10 belongs) is due to transitions from the filled to the unfilled part of a single band as with the calculation of Fig. 6, we expect that the knee in Fig. 10 should move to lower energies at higher temperatures; at 62 K we believe it is masked by the quasielastic, Rayleigh line.

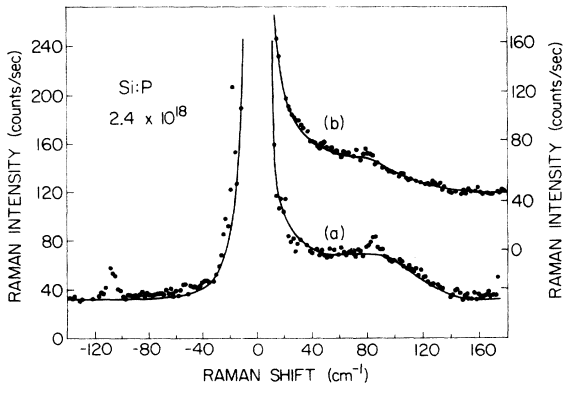

FIG. 8. Some details of the Raman spectrum of a Si:P sample just below the metal-insulator transition. (a) Stokes and anti-Stokes spectra at "$T = 20$ K" determined by a thermocouple. From ratios of Stokes to anti-Stokes intensities the true temperature is estimated to be about 36 K. The peaks at -107, -18, and +84 cm^{-1} are fluorescence lines from the YAlG : Nd laser. (b) Stokes spectrum at "$T = 63$ K" as determined by a thermocouple.

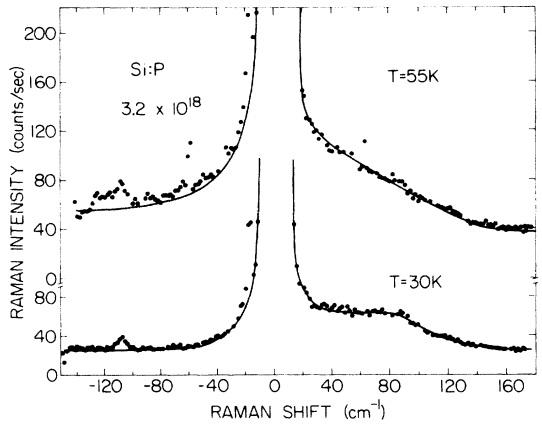

FIG. 9. Some details of the Raman spectrum of a Si:P sample very close to the metal-insulating transition. The temperatures were determined by ratios of Stokes to anti-Stokes Raman intensities. The peaks at -107 and -18 cm^{-1} are nonlasing fluorescence lines from the YAlG : Nd laser.

The Stokes and anti-Stokes spectra of a sample clearly in the insulating regime are shown in Fig. 11. The growth of the anti-Stokes line with temperature is as expected.

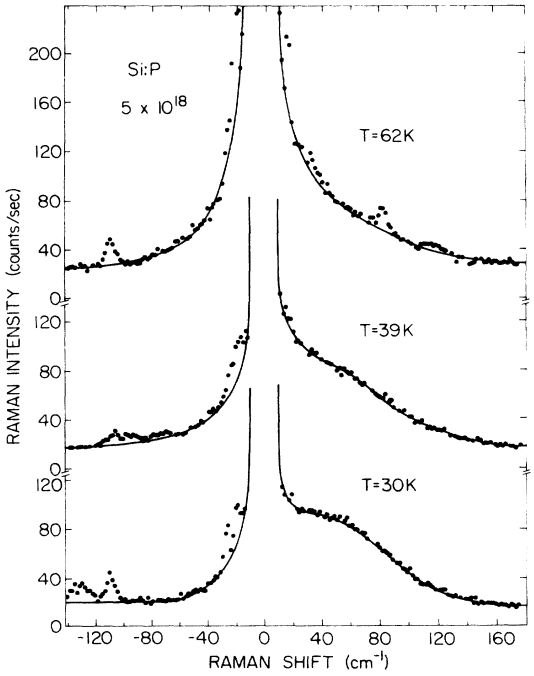

FIG. 10. Some details of the Raman spectrum of a Si:P sample above the metal-insulating transition. The temperatures were determined by ratios of Stokes to anti-Stokes Raman intensities. The peaks at -107, -18, and +84 cm^{-1} are fluorescence lines from the YAlG : Nd laser.

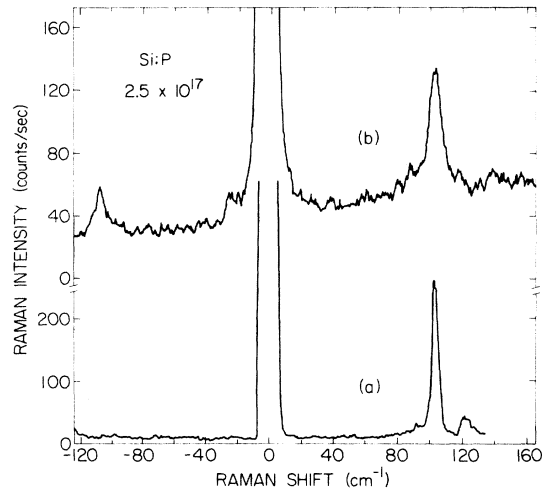

FIG. 11. Stokes and anti-Stokes Raman spectra of a lightly doped Si:P sample. (a) "$T = 15$ K" as determined by thermocouple. (b) "$T = 62$ K" as determined by thermocouple. From the ratio of Stokes to anti-Stokes intensities the actual temperature was estimated to be 75 K.

E. Sum rule for valley-orbit Raman intensity

We have measured the integrated Raman intensity for all our samples by measuring the area under the spectrum for each sample and calibrating it with respect to the strength of the 523-cm^{-1} zone-center optical phonon. We find that this integrated strength does not remain proportional to n_d throughout the range of concentrations studied; it drops as n_d increases. Below we derive a sum rule valid for all concentrations for an integral over the spectrum. It shows that the gross features of the spectrum are dominated by the intervalley potential of the donor atoms.

For the donor concentrations used here, the electrons are strongly influenced by the potential from the random distribution of donors. The existing theories of light scattering by a many-component electron plasma in a semiconductor neglect the influence of the donors.[37-39] Our sum rule includes this effect exactly. The cross section for Raman scattering by electron density fluctuations in a many-valley semiconductor can be written[37]

$$\frac{d^2\sigma}{d\omega\, d\Omega} = r_0^2 \frac{\omega_R}{\omega_L} \sum_f \sum_{ll'} \mu_l \mu_{l'} \langle f|\rho_l(q)|i\rangle \times \langle i|\rho_{l'}^\dagger(q)|f\rangle\, \delta(\omega_{fi} - \omega), \tag{34}$$

where

$$\mu_l = \vec{\eta}_L \cdot \vec{\mu}_l \cdot \vec{\eta}_R \tag{35}$$

and

$$\rho_l(q) = \int e^{i\vec{q}\cdot\vec{r}}\, \psi_l^\dagger(r)\, \psi_l(r)\, d^3r . \tag{36}$$

The $\psi_l(r)$ are field operators obeying the usual anticommutation relations. $\rho_l(q)$ is a number density fluctuation operator for valley l. Now we define a spectral function $\hat{S}(q,\omega)$:

$$\hat{S}(q,\omega) = \frac{\omega_L}{r_0^2 \omega_R} \frac{d^2\sigma}{d\omega\, d\Omega} = Av_i \sum_f \sum_{ll'} \mu_l \mu_{l'} \times \langle f|\rho_l(q)|i\rangle \langle i|\rho_{l'}^\dagger(q)|f\rangle \times \delta(\omega_{fi} - \omega). \tag{37}$$

Then by arguments similar to those of Nozieres and Pines[42] extended to finite temperatures, we find

$$\int_0^\infty \frac{\hat{S}(q,\omega)\omega\, d\omega}{1+n(\omega)} = Av_i \sum_f \sum_{ll'} \mu_l \mu_{l'} \langle [[\rho_l(q), H], \rho_{l'}^\dagger(q)]\rangle_T . \tag{38}$$

Here $\langle\ \rangle_T$ denotes a thermal average at temperature T, and $n(\omega)$ is the Planck function. We write the total Hamiltonian H in Eq. (38) as

$$H = V_C + V_{ee} + T + V_{sr} . \tag{39}$$

V_C is the Coulomb potential due to the donor nuclei, V_{ee} the electron-electron Coulomb interaction, and T the kinetic energy. V_{sr} is a short-range potential responsible for the valley-orbit splitting and is approximated by

$$V_{sr} = -V_0 \sum_R \psi_{A1}^\dagger(R;R)\psi_{A1}(R;R), \tag{40}$$

where ψ_{A1} is the field operator for the fully symmetric $1s(A_1)$ state of a donor at $\vec{R}$:

$$\psi_{A1}(r;R) = \frac{1}{\sqrt{v}} \sum_{l=1}^{v} e^{-i\vec{k}_l\cdot\vec{R}} \psi_l(\vec{r}). \tag{41}$$

The double commutator in Eq. (38) can be evaluated directly.[43] V_C commutes with $\rho_l(q)$, as does V_{ee}. The contributions of T and V_{sr} to the right-hand side of Eq. (38) may be computed directly. The respective contributions give two independent terms:

$$\int_0^\infty \frac{\hat{S}(q,\omega)\omega\, d\omega}{1+n(\omega)} = N \sum_{l=1}^{v} \frac{(\mu_l)^2}{v} \frac{\hbar}{2m} (\vec{q}\cdot\vec{\mu}_l\cdot\vec{q}) + \frac{N}{2v^2} \sum_{ll'} (\mu_l - \mu_{l'})^2 V_0 P_{cc} . \tag{42}$$

Here

$$P_{cc} = N^{-1} \sum_R \langle \psi_{A1}^\dagger(R;R)\psi_{A1}(R;R)\rangle_T \tag{43}$$

is the average number of electrons in the central cell of a donor. Use of Eq. (40) allows the following replacement in the second term in Eq. (42):

$$V_0 = \hbar\omega_{VO}/P_{cc}^{is}\,, \tag{44}$$

where P_{cc}^{is} is the value of P_{cc} for an isolated neutral donor in its $1s(A_1)$ ground state and $E_{VO} = \hbar\omega_{VO}$ is the valley-orbit splitting. Equations (42)–(44) state the *sum rule for* VO *Raman scattering*.

Equations (42) and (43) then give for E polarization geometry in silicon

$$N^{-1}\int_0^\infty \frac{\hat{S}(q,\omega)\omega\, d\omega}{1+n(\omega)} = \frac{(\mu_\parallel - \mu_\perp)^2}{6}\left(\frac{hq^{*2}}{2m} + \frac{\omega_{VO}P_{ee}}{P_{cc}^{is}}\right). \tag{45}$$

The parameter q^* is given by

$$q^{*2} = (\vec{q}\cdot\vec{\mu}_l\cdot\vec{q}) \tag{46}$$

for valleys l along $\pm x$ or $\pm y$ cube axes. For the conditions of our experiment, we find

$$\hbar q^{*2}/2m = 0.12\ \text{cm}^{-1}. \tag{47}$$

Since $\omega_{VO} = 105\ \text{cm}^{-1}$, the second, or intervalley scattering, term in Eq. (45) will dominate the sum rule as long as P_{ee}/P_{cc}^{is} is greater than about 10^{-2}.

We have computed values for the left-hand side of Eq. (42) for our Raman data of Figs. 2(a)–(g), together with data taken on samples of Figs. 2(h)–(j) with 5 W of unpolarized laser power, using the strength of the 523-cm^{-1} Raman-active $k=0$ phonon mode as an internal calibration. Special care was not taken to keep the cathode of the photomultiplier tube at the same temperature for all our data runs; thus its relative sensitivity in the phonon and valley-orbit spectral regions was not well-controlled, and the internal calibration using the phonon is only approximate. The results are shown in Fig. 12. The scatter is probably due to the effect mentioned above and due to difficulties in drawing a consistent base line. There seems to be a decrease of about a factor of four in the integrated spectrum, in the sense of Eq. (45), over the concentration range of our measurements. According to Eq. (45) this implies that P_{ee} has dropped to $\frac{1}{4}$ of its value for isolated donors.

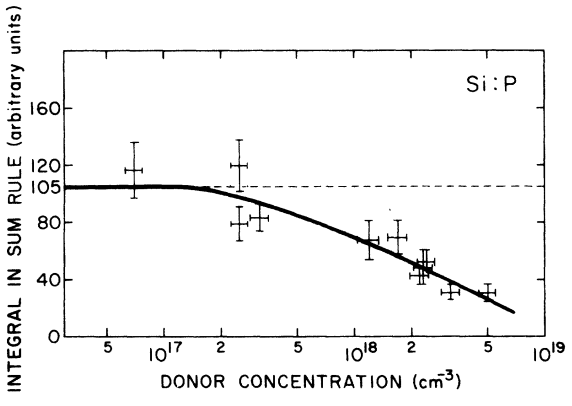

FIG. 12. Integral in the sum rule [Eq. (42)] as a function of donor concentration.

There are two explanations for the decrease of P_{cc}. Laser beam heating of the samples during the measurements for Fig. 12 caused the temperature of the crystals to rise from about 20 to 50 K over the concentration range of the experiments. Thermal activation could account for a decrease in P_{cc} since the ground-state $1s(A_1)$ orbital is the only one with appreciable amplitude at the donor sites. For instance if one assumes that there are five other orbitals 80 cm^{-1} above the $1s(A_1)$ orbitals, at $T = 50$ K one estimates a value of P_{cc}/P_{cc}^{is} of 0.6 from this effect. The other major cause of the decrease in central-cell occupation is probably due to delocalization of the $1s(A_1)$ orbitals as they interact with one another at high donor concentrations. An explicit, very approximate, calculation of this effect for n_d in the insulating regime has already been discussed.

V. OTHER EXPERIMENTS

A. *n*-Si samples doped with impurities other than phosphorus

In addition to Si:P crystals we have also studied several antimony and arsenic-doped silicon crystals. In Fig. 13 we show the Raman spectrum of a Si:Sb sample containing approximately 7×10^{16} antimony atoms/cm^3. This spectrum was taken with a 1.0795-μm-$YAlO_3:Nd^{3+}$: laser. The line at 98.2 cm^{-1} is the valley-orbit transition due to Sb

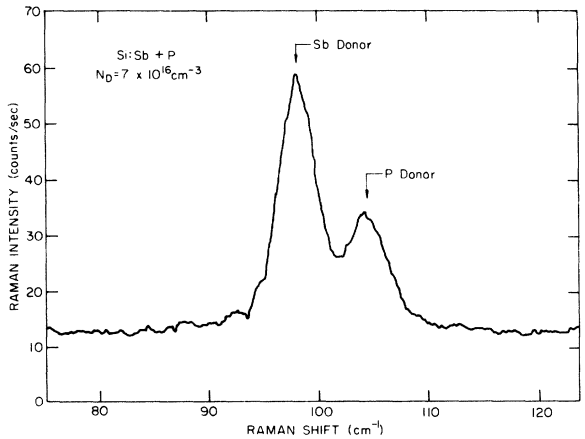

FIG. 13. Raman spectrum of a Si:Sb + P crystal with $n_d = 7\times10^{16}\ \text{cm}^{-3}$. "$T = 15$ K" as measured with a thermocouple. The scattering geometry was $z(xx+xz)y$ with $\vec{x}\,||\,[100]$, $\vec{y}\,||\,[011]$, and $\vec{z}\,||\,[01\bar{1}]$.

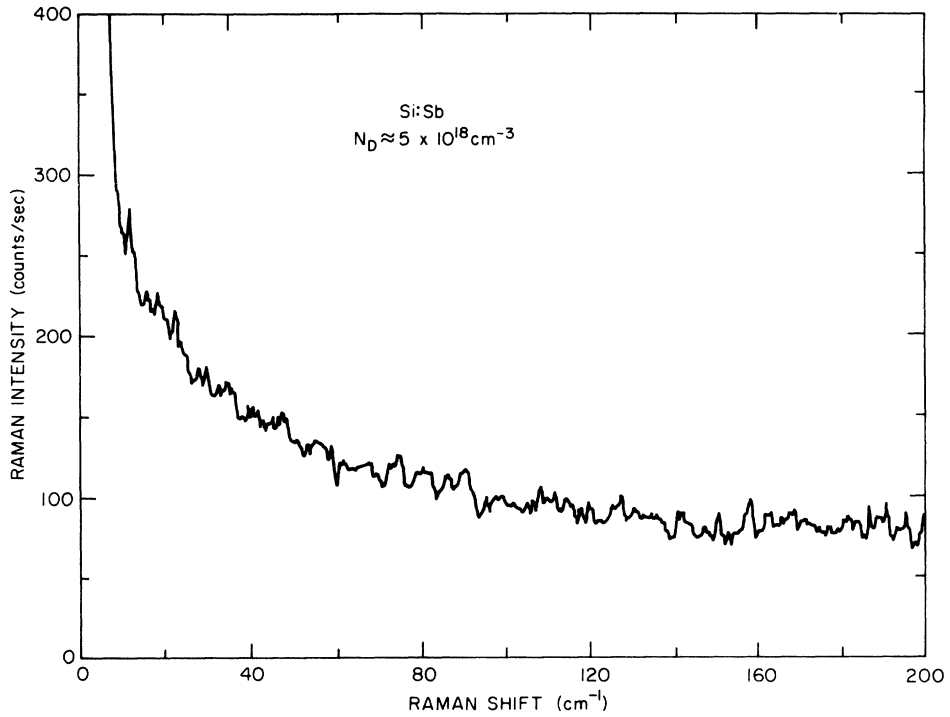

FIG. 14. Raman spectrum of Si:Sb with $n_d = 5 \times 10^{18}$ cm^{-3}. "$T = 23$ K" as measured with a thermocouple, but the actual temperature was probably about 50 K. The scattering geometry was the same as in Fig. 2.

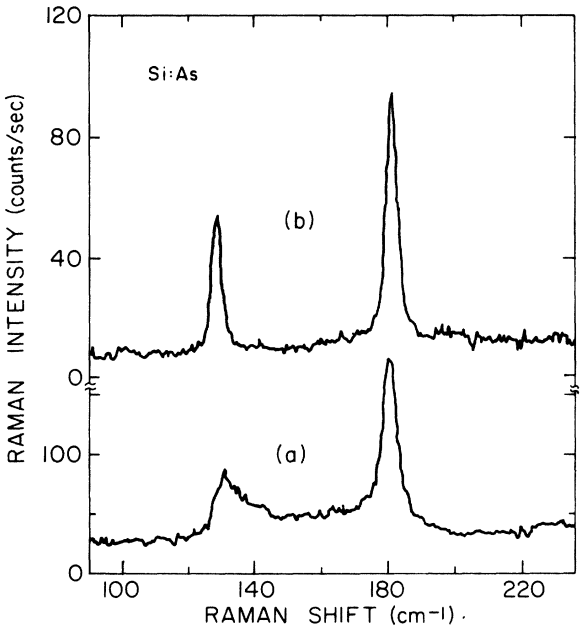

FIG. 15. Raman spectra of two Si:As crystals. (a) $n_d = 9.5 \times 10^{17}$ cm^{-3}, "$T = 19$ K". (b) $n_d = 6.5 \times 10^{17}$ cm^{-3}, "$T = 23$ K". The "T" values were measured with a thermocouple and are about 10 K too low. The scattering geometry was z (all, all)y with $\vec{x} \parallel [110]$, $\vec{y} \parallel [1\bar{1}0]$, and $\vec{z} \parallel [001]$.

donors. The energy of this $1s(A_1) \rightarrow 1s(E)$ transition agrees well with its previously published values.[44] The weaker peak at 104.5 cm^{-1} is due to the presence of some phosphorous in the sample. The relative strengths of the two peaks compare well with the concentrations of the two dopants as determined by mass-spectroscopic analysis. Figure 14 shows the Raman spectrum of a more heavily doped Si:Sb sample. Here the Sb concentration is 5×10^{18} cm^{-3}. This spectrum appears similar to that obtained for the "metallic" Si:P sample containing 5×10^{18} cm^{-3} impurity atoms. This is to be expected. In fact, since the ionization energy of Sb donors in silicon is smaller than that of P donors, the critical concentration n_c required for metallic behavior should be smaller for Si:Sb than for Si:P.[45]

In Figs. 15 and 16 we show the Raman spectra of three arsenic doped silicon samples. The $1s(A_1) \rightarrow 1s(E)$ transition is seen at 180 cm^{-1}. We observe that the line becomes broader with increasing impurity concentration. The asymmetric nature of the broadening, as observed in Si:P samples, is also seen here, particularly in the $n_d = 1.7 \times 10^{18}$-cm^{-3} sample. The line at 130 cm^{-1} is a mystery to us. We have not been able to attribute it to any known impurity in silicon. Owing

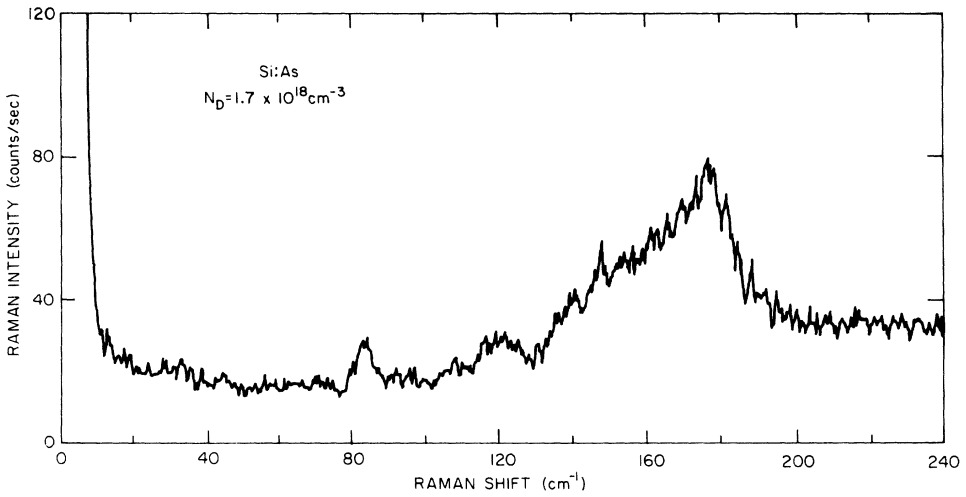

FIG. 16. Raman spectrum of Si:As with $n_d = 1.7\times10^{18}$ cm^{-3}. "T=24 K" as measured with a thermocouple. The scattering geometry was the same as in Fig. 15. The peak at 84 cm^{-1} is a laser fluorescence line.

to excessive absorption at the laser frequency, we could not study more heavily doped Si:As samples.

B. *p*-type silicon samples

In their experiments on zinc- and magnesium-doped gallium phosphide, Henry *et al.*[1] reported several Raman transitions. Some of these transitions, shown in Fig. 17, can be understood in terms of an effective-mass treatment of the acceptor states. The acceptor ground state is constructed from Bloch functions belonging to the fourfold degenerate $p_{3/2}(\Gamma_8)$ valence-band maximum multiplied by appropriate envelope functions. Transition A, which was observed extremely close to the laser line, can be attributed to transitions

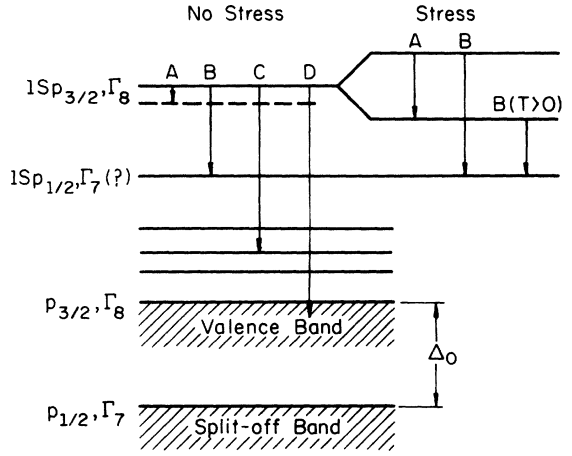

FIG. 17. Schematic representation of acceptor Raman transitions. Adapted from Ref. 1.

between the two Kramers doublets of this ground state split by a residual stress in the sample. From stress and temperature dependence of line B,[5] it was concluded that the final state for this transition should be Γ_6 or Γ_7. Bands C and D can be thought of as transitions to higher bound states and the valence band, respectively. Wright and Mooradian[2] observed a B-type line of T_2 symmetry in boron-doped silicon and found its behavior under stress[4] to be similar to that of the B transition in gallium phosphide.[5]

Klein[39] has given an outline of a theory of the Raman cross section for the A and B transitions in acceptors. He finds that both the A and B lines have both E and T_2 components. For the B transition, assuming it is $1Sp_{3/2}(\Gamma_8^+) \rightarrow 1Sp_{1/2}(\Gamma_7^+)$, he finds the following values of the E and the T_2 components. The coefficients are approximate, but the ratio of the two cross sections is correct within the effective-mass approximation:

$$\frac{d\sigma}{d\Omega(E)} = \tfrac{1}{3}r_0^2 R_{12}^2 \left(\frac{2m(L-M)}{\hbar^2}\right)^2 , \tag{48}$$

$$\frac{d\sigma}{d\Omega(T_2)} = \tfrac{1}{3}r_0^2 R_{12}^2 \left(\frac{2mN}{\hbar^2}\right)^2 . \tag{49}$$

Here r_0 is the classical radius of the electron and R_{12} is the resonance enhancement factor defined below Eq. (14). The dimensionless quantities $2m|L-M|/\hbar^2$ and $2m|N|/\hbar^2$ are defined by Dresselhaus *et al.*[46] and equal 2.25 and 9.36, respectively, for silicon.[47] Thus, the T_2 component should be 17.3 times stronger than the E component.

We have studied the Raman spectra of two boron-doped silicon crystals. In Fig. 18 we show the

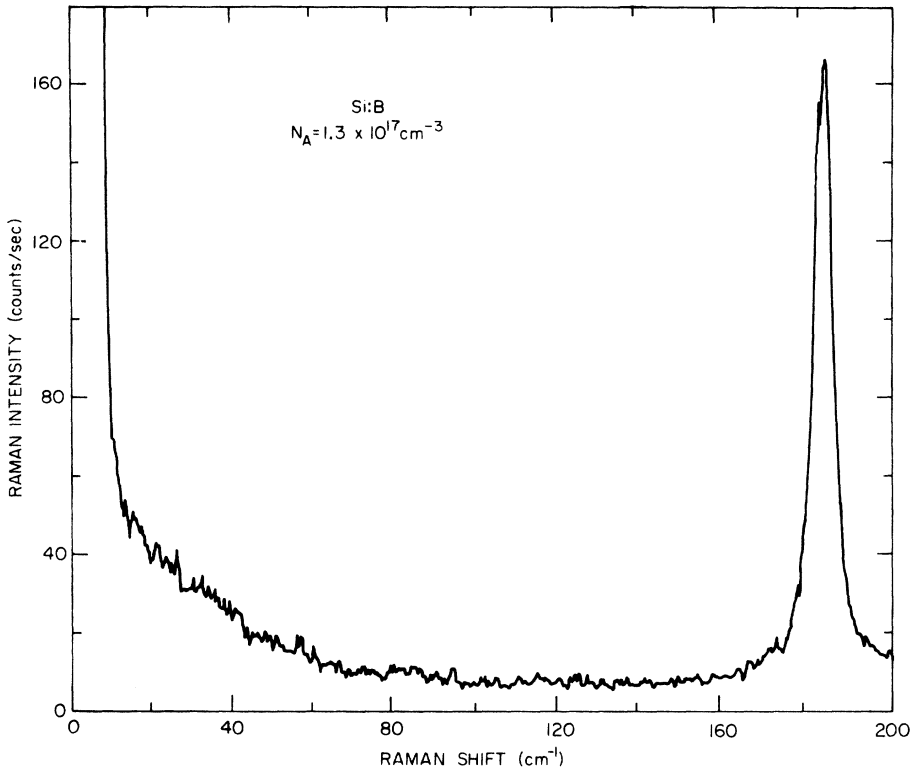

FIG. 18. Raman spectrum of Si:B with $n_a = 1.3 \times 10^{17}$ cm^{-3}. "$T = 22$ K" as measured with a thermocouple. Owing to laser beam heating the actual sample temperature probably rose to about 35 K.

spectrum obtained with a crystal containing approximately 1.3×10^{17}-cm^{-3} boron impurities. It was taken at a measured temperature of 22 K, but due to laser beam heating, the actual temperature, determined from the ratio of Stokes and anti-Stokes spectra, was approximately 35 K. The sharp line at 184 cm^{-1} (22.8 meV) is the B transition. The continuum starting near the laser line and extending to ~85 cm^{-1} resembles the single-particle spectrum seen in heavily doped n-type silicon crystals. Since acceptor states are derived from near the top of the valence band which is at $k = 0$, we do not think intervalley fluctuation is responsible for this continuum. Transition A (Fig. 17) between pairs of Kramers doublets of the ground state split by random stresses could be a possible explanation for this spectrum. We have also studied a Si:B sample with an impurity concentration of 2.4×10^{16} cm^{-3}. In this sample we see the sharp B transition at 184 cm^{-1}, as in the more heavily doped crystal, but the continuum is much weaker. With this sample we also tried to measure the relative strengths of the E and T_2 components. The E component was so weak that it was difficult to get a reliable value of the ratio $[d\sigma/d\Omega(T_2)]/[d\sigma/d\Omega(E)]$. Our rough estimates indicate that this value is at least 3.4, not inconsistent with Klein's theory.[39]

We have tried unsuccessfully to find a B-type transition in the Raman spectra of gallium- and aluminum-doped silicon samples. In Fig. 19 we show the Raman spectrum of a Si:Ga sample with $n_a = 6.5 \times 10^{17}$ cm^{-3}. No sharp acceptor transition is seen, but the continuum extends to about 30 meV. In a Si:Al sample with $n_a \sim 5 \times 10^{16}$ cm^{-3}, no discrete acceptor transition was seen, and the continuum was very much weaker than that seen in the gallium-doped crystal. We do not understand the absence of the B line in Si:Ga and Si:Al.[48] The continuum of Fig. 19 could be attributed to transition A, as in the case of Si:B (Fig. 18).

VI. SUMMARY

We have studied the Raman spectra of silicon single crystals doped with phosphorus and other n-type impurities as a function of impurity concentration. The $1s(A_1) \rightarrow 1s(E)$ valley-orbit line broadens rapidly and asymmetrically as the impurity concentration n_d increases. As n_d approaches the critical value n_c for the metal-insulator transition a continuum due to intervalley fluctuations starts appearing as a background. This single-particle-type spectrum grows in strength with increasing

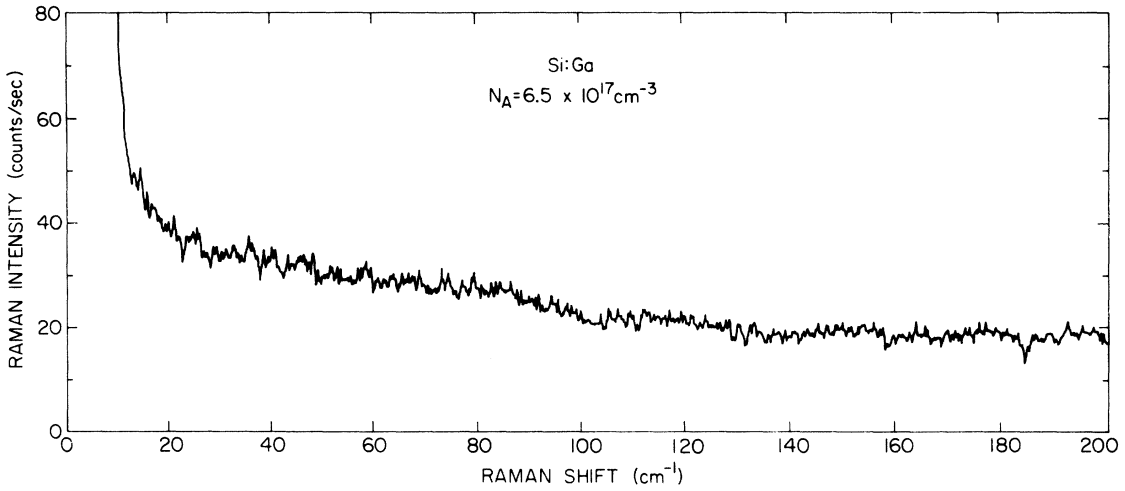

FIG. 19. Raman spectrum of Si:Ga with $n_a = 6.5\times10^{17}$ cm^{-3}. "$T = 23$ K" as measured with a thermocouple.

n_d and above n_c it completely dominates the spectrum. The valley-orbit line broadens beyond recognition as the impurity concentration reaches n_c or perhaps just before.

Using the notion that molecular bonding alters the valley-orbit splitting, we have calculated the line shape of the $1s(A_1) \rightarrow 1s(E)$ transition in the insulating regime. The main features of the valley-orbit line are understood qualitatively within the framework of this theory. For the single-particle spectrum in the metallic regime we have proposed a single-band random-transition model that reproduces several features of the actual data.

A sum rule valid for all concentrations has been derived for an integral over the spectrum. It shows that most of the Raman strength results from intervalley scattering processes due to the short-range part of the donor potential.

A search has been made for acceptor transitions in p-type silicon. We have observed a low-energy continuum for boron, gallium, and aluminum impurities, but the sharp B-type transition was seen only in Si:B.

ACKNOWLEDGMENTS

We wish to thank B. G. Streetman, G. E. Anner, C. T. Sah, and P. Handler of the University of Illinois, Urbana and K. P. Gupta of Monsanto Corp., St. Peters, Mo. for their donation of some of the samples used in this study. We also thank Robert Field for taking the absorption data of Fig. 1b. Special thanks go to S. A. Solin for suggesting that the heavily doped donor spectra would be sensitive to temperature.

*Supported in part by the NSF under grant No. GH-33757 and in part by the Advanced Research Projects Agency of the Department of Defense and monitored by the Air Force Office of Scientific Research under contract No. F44620-75-C-0091.

†Present address: Dept. of Electrical Engineering, Massachusetts Institute of Technology, Cambridge, Mass. 02139.

[1]C. H. Henry, J. J. Hopfield, and L. C. Luther, Phys. Rev. Lett. 17, 1178 (1966).

[2]G. B. Wright and A. Mooradian, Phys. Rev. Lett. 18, 608 (1967).

[3]G. B. Wright and A. Mooradian, Bull. Am. Phys. Soc. 13, 479 (1968).

[4]G. B. Wright and A. Mooradian, in *Proceedings of the Ninth International Conference on the Physics of Semiconductors, Moscow* (Nauka, Leningrad, 1968), p. 1067.

[5]D. D. Manchon, Jr., and P. J. Dean, in *Proceedings of the Tenth International Conference on the Physics of Semiconductors, Cambridge, Massachusetts*, edited by S. P. Keller, J. C. Hensel, and F. Stern (U.S. AEC, Oak Ridge, Tenn. 1970), p. 760.

[6]P. J. Colwell and M. V. Klein, Phys. Rev. B 6, 498 (1972).

[7]J. Doehler, P. J. Colwell, and S. A. Solin, Phys. Rev. B 9, 636 (1974).

[8]J. Doehler, P. J. Colwell, and S. A. Solin, Phys. Rev. Lett. 34, 584 (1975).

[9]A. Mooradian, in *Light Scattering Spectra of Solids*, edited by G. B. Wright (Springer-Verlag, New York, 1969), p. 285.

[10]D. C. Hamilton and A. L. McWhorter, in *Light Scattering Spectra of Solids*, edited by G. B. Wright (Springer-Verlag, New York, 1969), p. 309.

[11]J. F. Scott, T. C. Damen, J. Ruvalds, and A. Zawadowski, Phys. Rev. B 3, 1295 (1971).

[12]J. F. Scott, T. C. Damen, R. C. C. Leite, and J. Shah, Phys. Rev. B 1, 4330 (1970).
[13]C. K. N. Patel and E. D. Shaw, Phys. Rev. B 3, 1279 (1971).
[14]A. Mooradian, in *Laser Handbook*, edited by F. T. Arecchi and E. O. Shulz-DuBois (North-Holland, Amsterdam, 1972), Vol. II, p. 1309.
[15]G. Busch and H. Labhart, Helv. Phys. Acta 19, 463 (1946).
[16]C. Yamanouchi, K. Mizuguchi, and W. Sasaki, J. Phys. Soc. Jpn. 22, 859 (1967).
[17]H. Fritzsche, J. Phys. Chem. Solids 6, 69 (1958).
[18]H. Fritzsche, Phys. Rev. 125, 1552 (1962).
[19]W. Sasaki and R. de Bruyn Ouboter, Physica (Utr.) 27, 877 (1961).
[20]Y. Katayama and S. Tanaka, Phys. Rev. 153, 873 (1967).
[21]D. M. Finlayson and A. G. Mathewson, J. Phys. Chem. Solids 28, 1501 (1967).
[22]J. F. Woods and C. Y. Chen, Phys. Rev. 135, A1463 (1964).
[23]R. K. Sundfors and D. F. Holcomb, Phys. Rev. 136, A810 (1964).
[24]G. C. Brown and D. F. Holcomb, Phys. Rev. B 10, 3394 (1974).
[25]G. Feher, Phys. Rev. 114, 1219 (1959).
[26]S. Maekawa and N. Kinoshita, J. Phys. Soc. Jpn. 20, 1447 (1965).
[27]J. Bethin, T. G. Castner, and N. K. Lee, Solid State Commun. 14, 1321 (1974).
[28]J. R. Marko, J. P. Harrison, and J. D. Quirt, Phys. Rev. B 10, 2448 (1974).
[29]J. Doehler, Phys. Rev. B 12, 2917 (1975).
[30]W. Kohn, in *Solid State Physics*, edited by F. Seitz and D. Turnbull (Academic, New York, 1957), Vol. 5, p. 257.
[31]P. J. Colwell, Ph.D. thesis (University of Illinois, Urbana, 1971) (unpublished).
[32]W. P. Dumke, Phys. Rev. 118, 938 (1960).
[33]J. Hubbard, Proc. R. Soc. Lond. A 276, 238 (1963).
[34]J. Hubbard, Proc. R. Soc. Lond. A 281, 401 (1964).
[35]K. Jain, Ph.D. thesis (University of Illinois, Urbana, 1975) (unpublished).
[36]S. Chandrasekhar, Rev. Mod. Phys. 15, 1 (1943).
[37]P. M. Platzman, Phys. Rev. 139, A379 (1965).
[38]S. V. Gantsevich, V. L. Gurevich, and R. Katilius, Zh. Eksp. Teor. Fiz. 57, 503 (1969) [Sov. Phys.-JETP 30, 276 (1970)].
[39]M. V. Klein, in *Light Scattering in Solids*, edited by M. Cardona (Springer-Verlag, Heidelberg, 1975).
[40]P. N. Butcher and N. R. Ogg, Proc. Phys. Soc. Lond. 86, 699 (1965).
[41]A. S. Barker and R. Loudon, Rev. Mod. Phys. 44, 18 (1972).
[42]P. Nozières and D. Pines, Phys. Rev. 109, 741 (1958).
[43]The exact many-valley form of the effective-mass wave equation has been given by W. D. Twose in: H. Fritzsche, Phys. Rev. 125, 1552 (1962). For slowly varying envelope functions, one can show that the intervalley contributions from V_c and T are small.
[44]P. Fisher and A. K. Ramdas, in *Physics of the Solid State*, edited by S. Balakrishna, M. Krishnamurthi, and B. Ramachandra Rao (Academic, New York, 1969), p. 149.
[45]M. N. Alexander and D. F. Holcomb, Rev. Mod. Phys. 40, 815 (1968).
[46]G. Dresselhaus, A. F. Kip, and C. Kittel, Phys. Rev. 98, 368 (1955).
[47]J. C. Hensel and G. Feher, Phys. Rev. 129, 1041 (1963).
[48]These negative results for Si:Ga and Si:Al were also found by G. B. Wright and A. Moordian (private communication).